J Mater Sci (2009) 44:2310–2319
DOI 10.1007/s10853-008-3020-4

FESTSCHRIFT IN HONOUR OF PROF T R ANANTHARAMAN ON THE OCCASION OF HIS 80TH BIRTHDAY

Mechanical, corrosion, and sliding wear behavior of intermetallics reinforced austenitic stainless steel composites

S. Balaji · A. Upadhyaya

Received: 9 April 2008 / Accepted: 26 September 2008 / Published online: 23 October 2008

Abstract The present work investigates the effect of supersolidus sintering and intermetallics (Ni_3Al, Fe_3Al) additions on the densification, mechanical, tribological, and electrochemical behavior of sintered austenitic (316L) stainless steels. The performances of the supersolidus liquid phase sintered (SLPS) compacts are compared with the conventional solid-state sintered (SSS) compacts of similar compositions. Correspondingly, the sintering was carried out at two different temperatures 1200 °C (SSS) and 1400 °C (SLPS). Supersolidus sintering results in significant improvement in densification, wear resistance, corrosion resistance, strength, and ductility in both straight as well as aluminide added composites.

Introduction

Powder metallurgy (P/M) has proven to be a cost-effective method for the manufacturing of large quantity of particulate reinforced metal matrix composites. The conventional solid-state sintered composites exhibited inferior densification. Previous studies on the solid-state sintered ceramic reinforced stainless steels showed that, the presence of higher amount of porosities in these composites overrides the positive effects of the hard reinforcement phases [1, 2]. Liquid phase sintering (LPS) is a widely used fabrication process in powder metallurgy to attain higher sintered densities. The presence of a liquid phase during sintering activates the sintering kinetics. Liquid phase during sintering can be obtained through a lower melting point second phase or by formation of a eutectic. In order to achieve significant advantage in densification through capillary force, a small initial particle size—often in the range of 1 μm or less—is required [3]. A variant to traditional liquid-phase sintering for coarser prealloyed powders is supersolidus liquid phase sintering (SLPS). SLPS involves heating a prealloyed powder between the solidus and liquidus temperature to form liquid phase. During SLPS, the liquid phase forms within the particles, causing each particle to fragment into individual grains. The fragmented particles undergo repacking. The resulting sintering rate is rapid once the liquid is formed due to capillary action [4, 5].

Powder metallurgy processing allows the microstructural modification with respect to the reinforcement size, shape, and placement. Pagounis and Lindroos [6] compared the mechanical, wear, and corrosion behavior of metal matrix composites prepared by hot isostatic pressing using various particulate reinforcements such as Al_2O_3, TiC, Cr_3C_2, and TiN with the corresponding unreinforced 316L stainless steel matrix. Al_2O_3 reinforcements exhibit a clean interface free from any diffusion alloying or reactions with the 316L matrix. At the interface, TiC reinforcements were found to occur as spherical precipitates, while the Cr_3C_2 reinforcements formed a thick layer. The composites reinforced with Al_2O_3 particles resulted in the least wear resistance, particularly at the higher volume fractions. This was attributed to the weak interface bonding of Al_2O_3 with the steel matrix, which caused spalling of the particles during wearing. Elsewhere, Datta and Upadhyaya [7] have reported that Cr_3C_2 addition is beneficial for increasing microhardness of sintered 316L. Near-full density was achieved for 316L composites with 2 wt.% CrB addition. Positive effects of reinforcing ceramic particles (Al_2O_3 and

S. Balaji · A. Upadhyaya (✉)
Department of Materials and Metallurgical Engineering,
Indian Institute of Technology, Kanpur 208016, India
e-mail: anishu@iitk.ac.in

Y_2O_3) along with the sintering activators (B_2Cr and BN) on the wear resistance of P/M austenitic 304L and 316L stainless steel were also reported by Velasco et al. [8] and Vardavoulias et al. [9]. Akhtar and Guo [10] reported that 50–70 wt.% TiC additions to stainless steel binder results in improved wear resistance. Elsewhere, Tjong and Lau [11, 12] have reported a significant improvement in the macrohardness, sliding wear, and abrasion wear resistance for 20 vol.% TiB_2 to 304L stainless steels. However, the major drawback of these particulate reinforced composites is their poor corrosion behavior compared to straight stainless steels. The poor interaction between the matrix and reinforcements promotes the onset of the corrosion attack. Recently, Shankar et al. [1, 13] have reported that Y_2O_3 addition marginally increases densification in 316L compacts in solid-state and supersolidus sintering condition. This finding was attributed to the interaction of Cr_2O_3 with the Y_2O_3 dispersoids. Subsequent analysis revealed no significant degradation of the corrosion resistance in 316L–Y_2O_3 composites as compared to straight 316L compacts. Jain et al. [2] have also observed similar interaction for yttrium aluminum garnet (YAG) additions to 316L and 434L stainless steels. The beneficial effects of supersolidus sintering and YAG additions on the corrosion behavior of 316L stainless steels were also reported by Balaji and Upadhyaya [14]. As compared to oxide and carbide reinforcements, aluminide-based intermetallics have shown better interaction with the stainless steel matrix [15–18]. It is envisaged that such an interaction results in enhanced corrosion resistance. Furthermore, the interaction can aid in smoother compositional variation which can assist in reducing localized (e.g. intergranular) corrosion. Velasco et al. [15] attributed the improved wear performance of the vacuum sintered TiAl reinforced 316L stainless steel composites to the reaction of TiAl with the 316L matrix which allowed higher degree of transformation of austenite to martensite during wear testing. Abenojar et al. [16, 17] reported a comparable wear resistance and improved corrosion resistance during salt spray test for the intermetallic reinforcements (Cr_2Al, $TiCr_2$) as compared to the carbide reinforcements.

The present work investigates the effect of aluminide (Ni_3Al and Fe_3Al) additions and supersolidus sintering on the densification, mechanical, tribological, and corrosion performance of sintered austenitic (316L) stainless steels.

Experimental procedure

Composite preparation

Austenitic 316L (C: 0.025; Si: 0.93; Mn: 0.21; Ni: 12.97; Cr: 16.5; Mo: 2.48; S: 0.008; P: 0.01; Fe: bal.) stainless steel powders for the present study were supplied by Ametek Specialty Metal Products (USA). The Ni_3Al and Fe_3Al powders (purity: >99.7%) were supplied by Xform Inc. (USA). Table 1 summarizes the characteristics of the as-received powders. The prealloyed 316L powders were mixed with 5 and 10 wt.% of Ni_3Al and Fe_3Al reinforcements in a turbula mixer (model: T2C, supplier: Bachofen, Basel, Switzerland) for 1 h. Cylindrical pellets (for densification and corrosion studies) and flat tensile bars as per MPIF specifications (for tensile and wear testing) were compacted from the mixed compositions at 600 MPa using a 50-ton capacity hydraulic press (model: CTM-50, supplier: FIE, Ichalkaranji, India) with floating die, using zinc stearate as a die wall lubricant. Compaction pressure was restricted to 600 MPa since application of larger force resulted in delamination in the green (as-pressed) parts. The as-pressed compacts were sintered in an $MoSi_2$ heated horizontal tubular sintering furnace (model: OKAY 70T-7, supplier: Bysakh, Kolkata, India) at a heating rate of 5 °C/min. At isothermal hold, the temperature was controlled within ±2 °C accuracy. Panda et al. [19] reported the onset of melt formation for the prealloyed 316L powder as 1383 °C based on the differential scanning calorimetry results. Hence, the supersolidus sintering was carried out at 1400 °C. The chosen supersolidus sintering temperature did not result in compact distortion of both 316L and 316L–aluminide composites. The performance of the supersolidus sintered compacts was compared with those sintered at 1200 °C corresponding to solid-state sintering. Sintering was carried out in hydrogen atmosphere (dew point: −35 °C) for 1 h.

Table 1 Characteristics of the as-received powders used in the present investigation

Property	Powder		
	316L	Ni_3Al	Fe_3Al
Supplier	Ametek	Xform	Xform
AD (g/cm^3)	2.7	3.9	3.5
Flow rate (s/50 g)	28	15	21
TD (g/cm^3)	8.06	7.5	6.72
Cumulative powder size (μm)			
D_{10}	10	36	39
D_{50}	46	50	54
D_{90}	85	68	74

AD apparent density, *TD* theoretical density

Characterization

The sintered density of the compacts was measured using Archimedes principle. The theoretical densities of the composites were calculated using inverse rule of mixtures

and all the density values are reported in terms of % theoretical density. Vickers bulk hardness measurements were performed on the polished surfaces of the composites at 5 kg load. The tribological response of the sintered composites was assessed using pin-on-disc wear testing machine (model: TR-20, supplier: DUCOM, Bangalore, India). The sintered samples in the form of cylindrical pins were tested against a hardened EN31 (AISI 52100) steel disc at 1 m/s sliding velocity. The cumulative wear rate of various compositions sintered in both conditions (SSS and SLPS) was calculated after 1000 m of sliding using the following expression [20]:

$$\text{Cumulative wear rate}\,(\text{mm}^3/\text{Nm}) = \frac{\Delta m}{\rho F S} \quad (1)$$

where Δm = weight loss after sliding (g); F = applied normal load (N); ρ = density, and S = sliding distance (m).

The electrochemical experiments were performed to assess the corrosion behavior of the composites using potentiostat (model: PC4, supplier: Gamry Instruments) on a CMS100 Framework. The Tafel experiments were performed in 3.56 wt.% NaCl solution freely exposed to air at 0.166 mV/s scan rate using a flat cell with standard three-electrode (reference, counter, and working) configuration. The reference electrode used for the present experiment was standard calomel electrode (SCE) saturated with saturated KCl and the sintered. All potentials were measured with respect to the SCE. Prior to the Tafel test, each sample was stabilized for about 3600 s in the solution to get a stable open circuit potential (OCP).

Results and discussion

Densification

Figure 1a shows the sintered density variation of the straight 316L and its aluminide added composites with sintering temperature. Supersolidus sintering results in improved sintered density in both straight 316L as well as 316L–aluminide composites. Addition of aluminides to 316L stainless steels marginally decreases the sintered density during solid-state sintering. In contrast, aluminide additions result in slight density improvement in supersolidus sintered 316L stainless steel compacts. The densification parameters (Ψ) of the sintered compacts have been calculated using the following expression:

$$\psi = \frac{\text{SD} - \text{GD}}{\text{TD} - \text{GD}} \quad (2)$$

where SD = sintered density, GD = green density, TD = theoretical density. The variation of densification parameter with sintering temperature for the straight 316L stainless steels and 316L–aluminide composites are shown in Fig. 1b. Significant improvement in the densification is observed for supersolidus sintered 316L stainless steel and 316L–aluminide composites. The addition of aluminides to 316L stainless steels did not affect the compressibility of the compacts. The green density variation for the aluminide additions is very minimal (83 ± 0.2%). So, the densification parameter also followed the similar trend as sintered density.

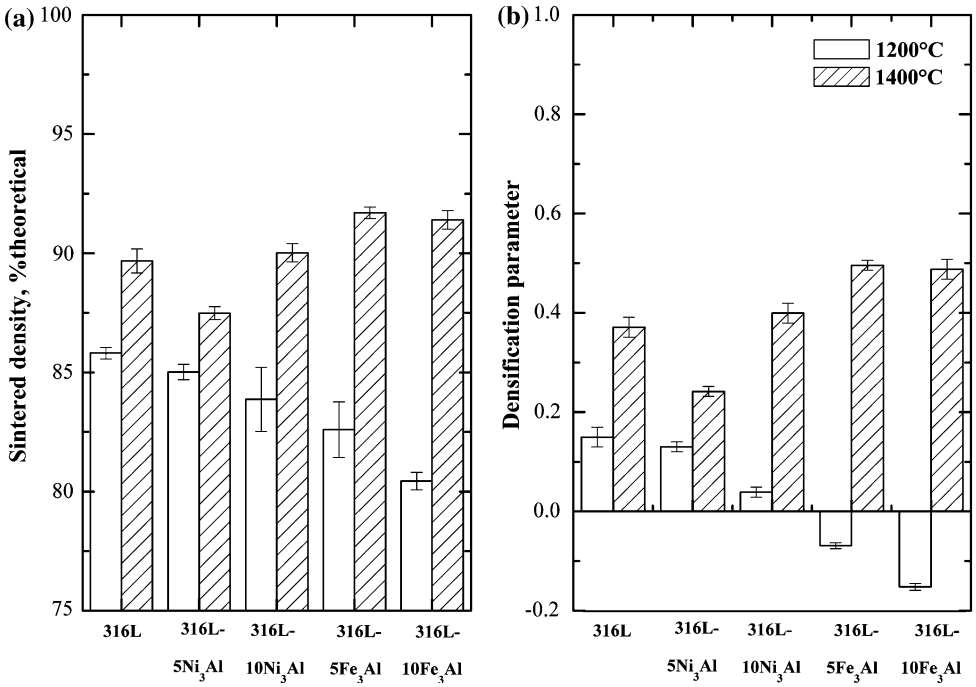

Fig. 1 Effect of sintering temperature on the **a** sintered density and **b** densification parameter of straight 316L and 316L–aluminide composites

Microstructural evolution

The optical micrographs of the straight 316L stainless steels and 316L–aluminide composites sintered at two different sintering conditions are given in Fig. 2. Clearly, the porosity level in the straight 316L stainless steels sintered at 1200 °C is higher when compared to 1400 °C sintered compacts. This correlates with the densification results shown in Fig. 1. The solid-state sintered stainless steels contain mostly irregular, intergranular pores. In contrast, the supersolidus sintered compacts contain predominantly intragranular and more rounded pores with a significant grain coarsening. The matrix porosity and average grain size are similar to that of straight stainless steels in both the sintering conditions. From the microstructure it is evident that the Ni_3Al and Fe_3Al retain their identity and appear as distinct phases which are surrounded by a dark rim. The EDAX analysis at the dark rim portion (316L–aluminide interface) confirmed the formation of oxides of aluminum. Similar observation was also reported by Abenojar et al. [16] for 316L–3 vol.% Cr_2Al when sintered at 1230 °C in H_2 atmosphere.

The elemental X-ray mapping of the 316L–Ni_3Al and 316L–Fe_3Al composites are given in Figs. 3 and 4, respectively. In all the cases, a rim of alumina forms at the 316L–aluminide interface. At lower temperatures the aluminide phase does not interact with the stainless steel matrix. However, at 1400 °C a noticeable interaction has been observed in both Ni_3Al and Fe_3Al added composites. In the 316L–Ni_3Al composites, considerable amount of Cr and Fe had diffused into the Ni_3Al phase. Similarly, in the case of 316L–Fe_3Al composites, considerable amount of Ni and Cr had diffused into the Fe_3Al phase. The interactions result in a uniform distribution of Cr, Ni, and Fe throughout the cross section of the composites. At lower sintering temperature (1200 °C), the lesser contact area between the aluminides and stainless steels account for the absence of interaction between them in terms of Cr diffusion across the interface. On the other hand, melt formation at supersolidus sintering conditions leads to better bonding between the aluminides and stainless steel. This results in the diffusion of Cr and Fe into the Ni_3Al and Cr and Ni into the Fe_3Al. Better densification of aluminide reinforced composites is attributed to both supersolidus sintering of the stainless steel matrix as well as the interaction between the matrix and aluminide reinforcements.

Mechanical behavior

The mechanical properties of the 316L stainless steels and 316L–aluminide composites sintered at 1200 and 1400 °C are reported in Table 2. As the sintering temperature increases both strength as well as ductility of compact increases. This can be attributed to greater densification at higher sintering temperature. Besides, it is a well-recognized fact that higher sintering temperature results in more pore rounding in steels. This reduces the stress concentration factor and contributes toward enhancement of mechanical properties.

The addition of aluminides to 316L stainless steel decreases the strength and ductility. The addition of 5 wt.% aluminides to 316L stainless steel causes a reduction in

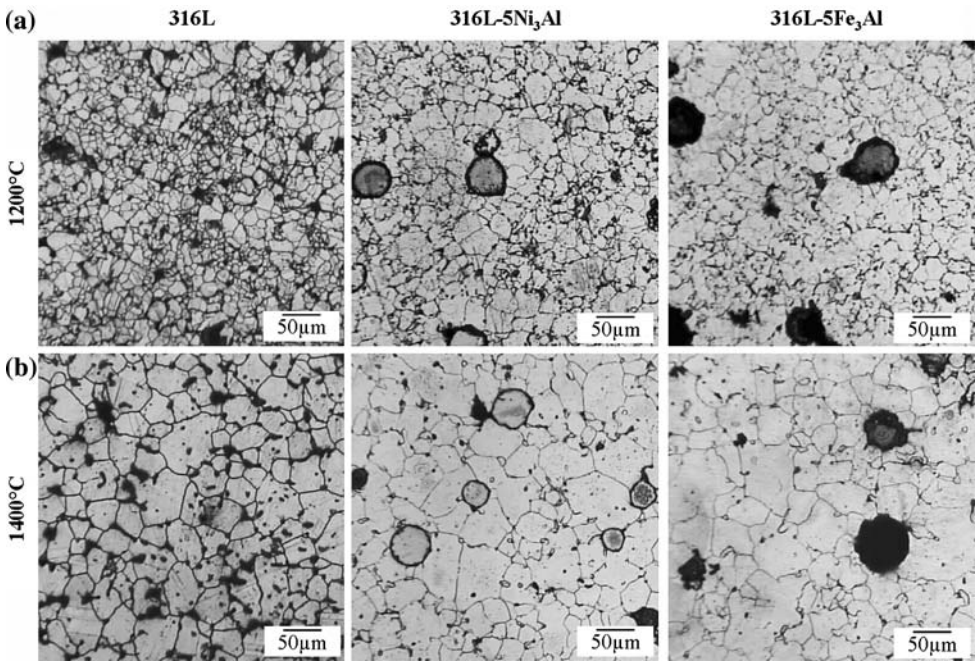

Fig. 2 Optical micrographs of straight 316L stainless steels and 316L–aluminide composites sintered at **a** 1200 °C and **b** 1400 °C

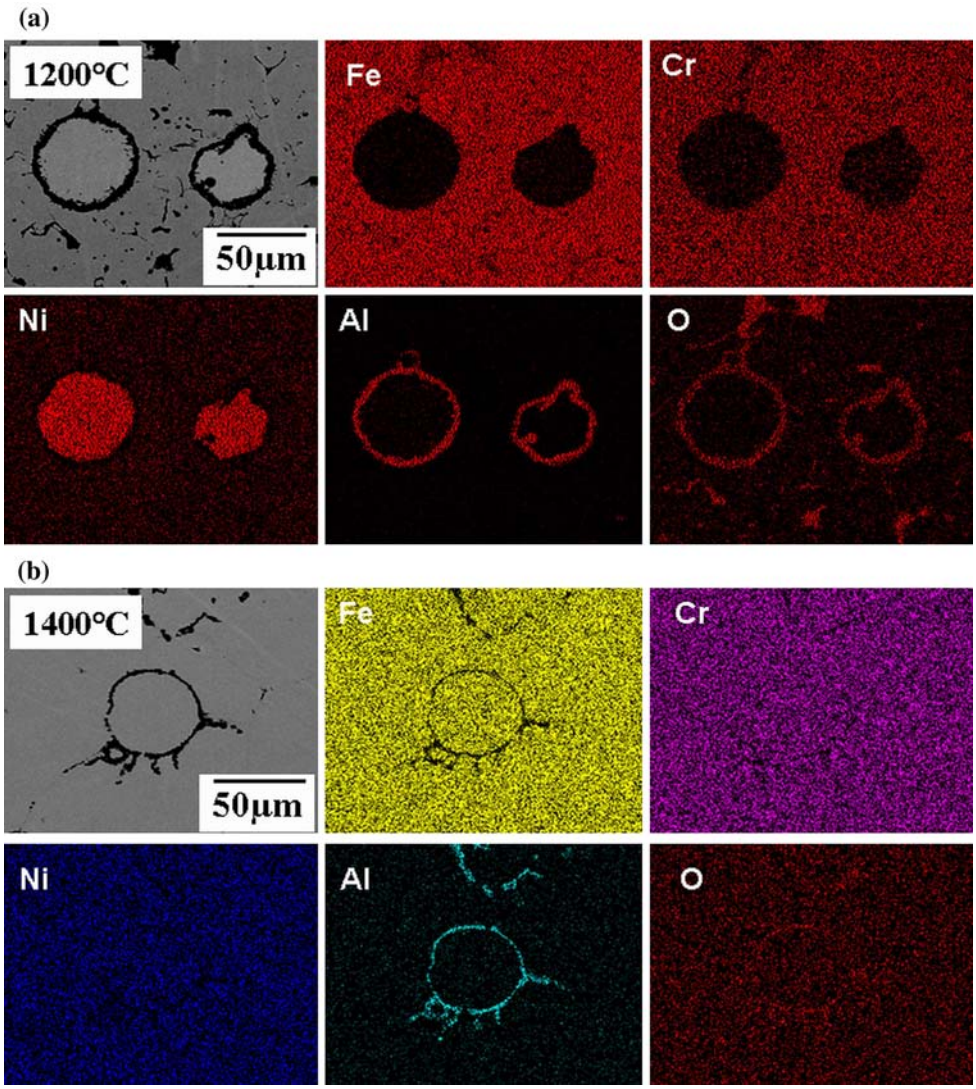

Fig. 3 Elemental mapping of 316L–Ni_3Al composite sintered at **a** 1200 °C and **b** 1400 °C

strength and ductility, but further addition to 10 wt.% increases the strength and ductility of 316L compacts. As compared to solid-state sintering, supersolidus sintering results in significant enhancement in the mechanical properties of 316L–aluminide composites. This can be attributed to matrix-reinforcement interaction induced solid-solution strengthening. The inferior densification corresponding to lower sintering temperature reduces the effective cross-sectional area over which the load is applied. This increases the effective stress level at the particle contacts which results in lower tensile properties. The fractographs shown in Fig. 5 too confirm the deformation at the interparticle neck regions indicated by smaller dimples. Despite its coarser grains the supersolidus sintered compacts had better mechanical properties. This can be attributed to the enhanced densification and solid-solution strengthening effects due to the matrix reinforcement interaction observed in the compacts sintered at 1400 °C. From the fractographs, it is evident that at lower sintering temperatures, the aluminide phase does not bear any load and it detaches as a complete particle while fracturing. The crack initiation starts at the stainless steel-aluminide interface. As the aluminide content increases, the effective load bearing cross section decreases, which results in lowering of strength. The hydrogen embrittlement of the aluminides is a well-known phenomenon [21]. The sintering in the hydrogen atmosphere could have embrittled the aluminide phase. The fracturing of the aluminide phase in compacts that were sintered at 1400 °C could be an outcome of the interactions observed with the reducing atmosphere (hydrogen). This however needs to be investigated further in more detail.

Figure 6 shows the bulk hardness variation of the sintered compacts with aluminide additions and sintering

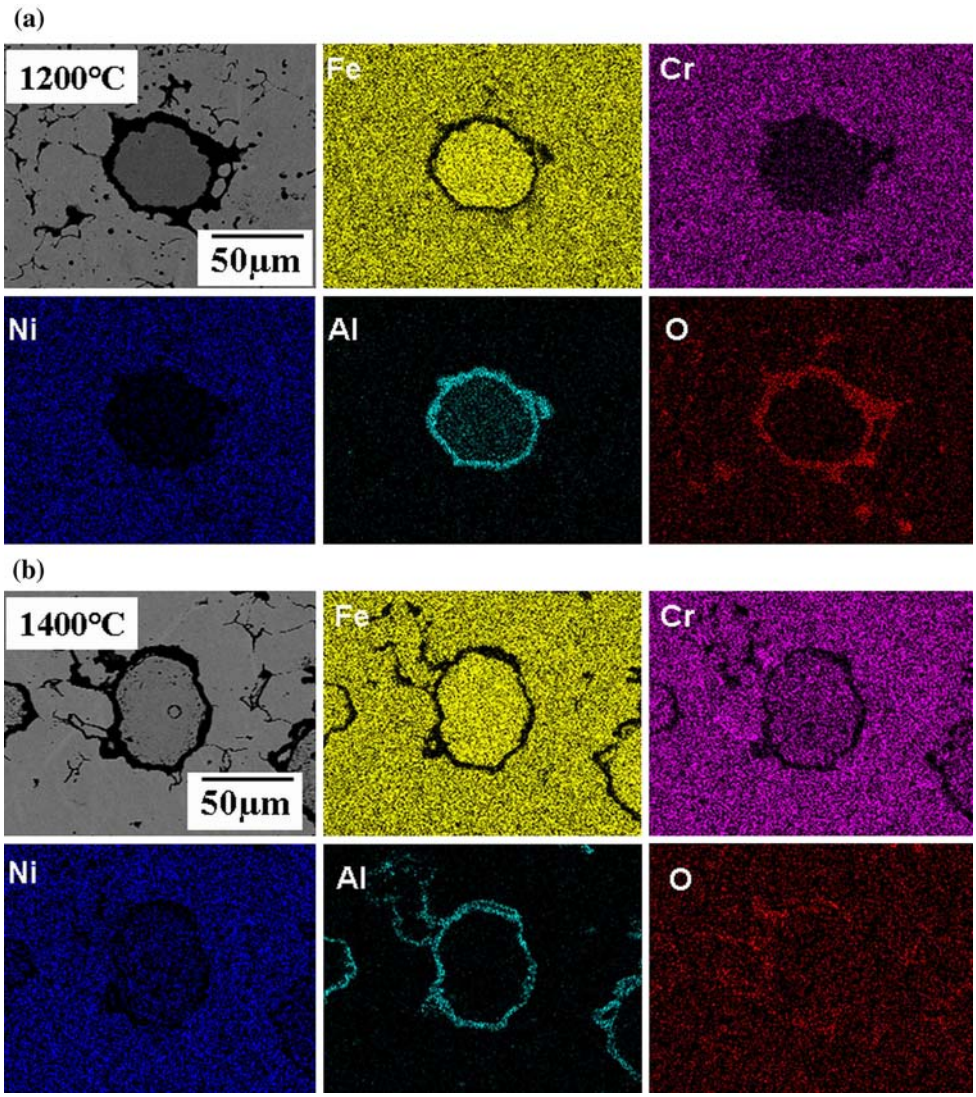

Fig. 4 Elemental mapping of 316L–Fe_3Al composite sintered at **a** 1200 °C and **b** 1400 °C

temperature. The bulk hardness of the sintered compacts increases with increase in sintering temperature. The increase in bulk hardness of the compacts with increase in the sintering temperature is attributed to better densification at higher temperatures. The improvement in bulk hardness of the aluminide added composites are marginally better than that of the straight stainless steels. This effect can be attributed to the chemical interaction between the stainless steel matrix and the aluminide dispersoid observed at higher sintering temperatures. The addition of both Ni_3Al and Fe_3Al to 316L stainless steels increases the bulk hardness of the stainless steels. As compared to Ni_3Al additions, Fe_3Al additions result in higher bulk hardness values. This effect is attributed to the higher hardness of the dispersoid particles. Fe_3Al dispersoid is having better hardness, and hence results in marginal improvement in bulk hardness than the Ni_3Al added composites.

Sliding wear behavior

The variation of wear volume with sliding distance for the 316L stainless steel and the 316L compacts with Ni_3Al and Fe_3Al addition is shown in Fig. 7a, b. Figure 7 clearly indicates that the wear resistance of straight stainless steel is only marginally affected by supersolidus sintering. In contrast, for 316L–aluminide composites, a wear resistance significantly increases in SLPS compacts. This implies better interfacial bonding/interaction between the stainless steel and the aluminides at high sintering temperature. The variation of cumulative wear rates with sintering temperature and aluminide additions is presented in Fig. 8 and follows the same trend as Fig. 7 with respect to sintering temperature and aluminide content. The wear rate decreases with increase in sintering temperature for all the sintered compacts. Furthermore, the addition of both Ni_3Al

Table 2 Tensile properties of 316L–aluminide composites

Sample	Theoretical density (g/cm^3)	Green density (g/cm^3)	Sintering temperature (°C)	UTS (MPa)	0.2% offset yield strength (MPa)	%Elongation	%Area reduction
Straight 316L	8.06	6.71	1200	207	167	5.9	2.5
			1400	363	145	47.8	19.8
316L–5Ni_3Al	8.03	6.65	1200	145	140	3.0	3.2
			1400	267	115	23.4	7.8
316L–10Ni_3Al	8.00	6.66	1200	172	135	6.1	2.8
			1400	320	122	33.5	13.9
316L–5Fe_3Al	7.98	6.60	1200	129	120	2.4	0.7
			1400	265	108	29.5	19.3
316L–10Fe_3Al	7.90	6.56	1200	92	81	2.7	0.8
			1400	351	188	33.8	20.2

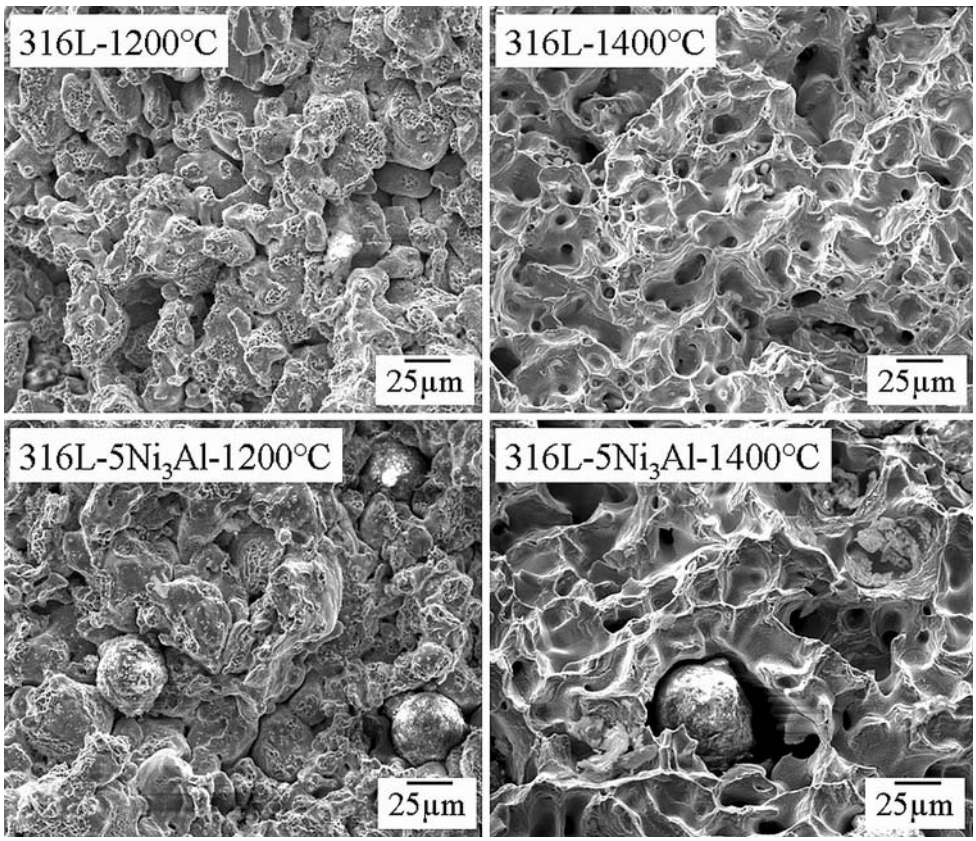

Fig. 5 Fractographs of straight 316L stainless steels and 316L–Ni_3Al composites sintered at 1200 °C and 1400 °C

and Fe_3Al to 316L stainless steel improves the wear resistance. This is in direct correlation with the bulk hardness values reported in Fig. 6.

Corrosion rate measurement

From the extrapolation of the Tafel curves (Fig. 9) the corrosion potential, E_{corr} (measured relative to SCE), Tafel slopes in the anodic and cathodic region (β_a and β_c, respectively), and corrosion current density (i_{corr}) were determined and are tabulated in Table 3. The corrosion rate was calculated using the following expression [22]:

$$\text{Corrosion rate (mmpy)} = 0.0033 \times \frac{e}{\rho} \times i_{corr} \quad (3)$$

where e = equivalent weight, ρ = theoretical density (g/cm^3), i_{corr} = corrosion current density (μA/cm^2). Irrespective of the aluminide type and the amount there is a

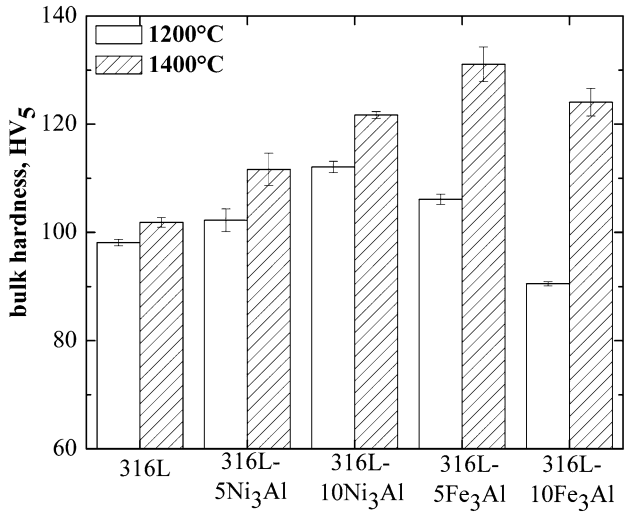

Fig. 6 Effect of aluminide additions and sintering temperature on the bulk hardness of 316L stainless steels

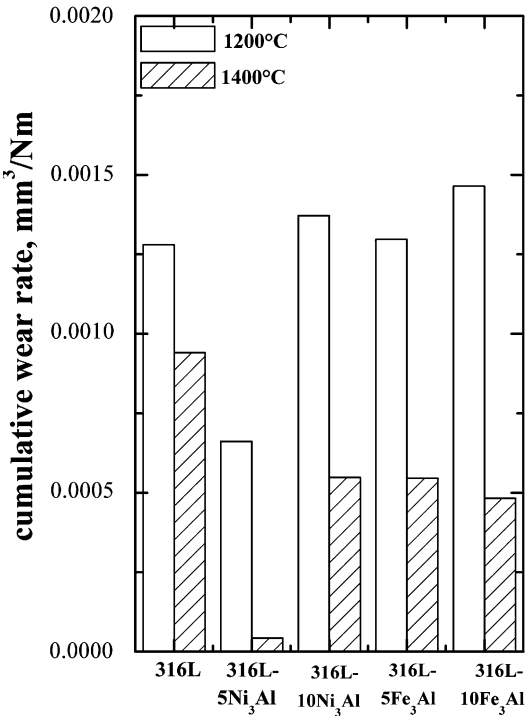

Fig. 8 Effect of aluminide addition and sintering temperature on the cumulative wear rate of 316L-based stainless steels

significant improvement in the corrosion resistance for the supersolidus sintered compacts as compared to the conventional solid-state sintered compacts. This can be attributed to the enhanced densification achieved by the 1400 °C sintered samples. Furthermore, Cr diffusion into the aluminide phases in the supersolidus sintered composites may also contribute toward improving the corrosion resistance. The addition of 5 wt.% Ni_3Al to 316L stainless steels improves the corrosion resistance in both solid-state as well as supersolidus sintered conditions. Similar improvement in corrosion resistance with 5 wt.% Ni_3Al addition was reported in 0.1N H_2SO_4 solution as well [18]. Higher amount of aluminide additions to 316L stainless

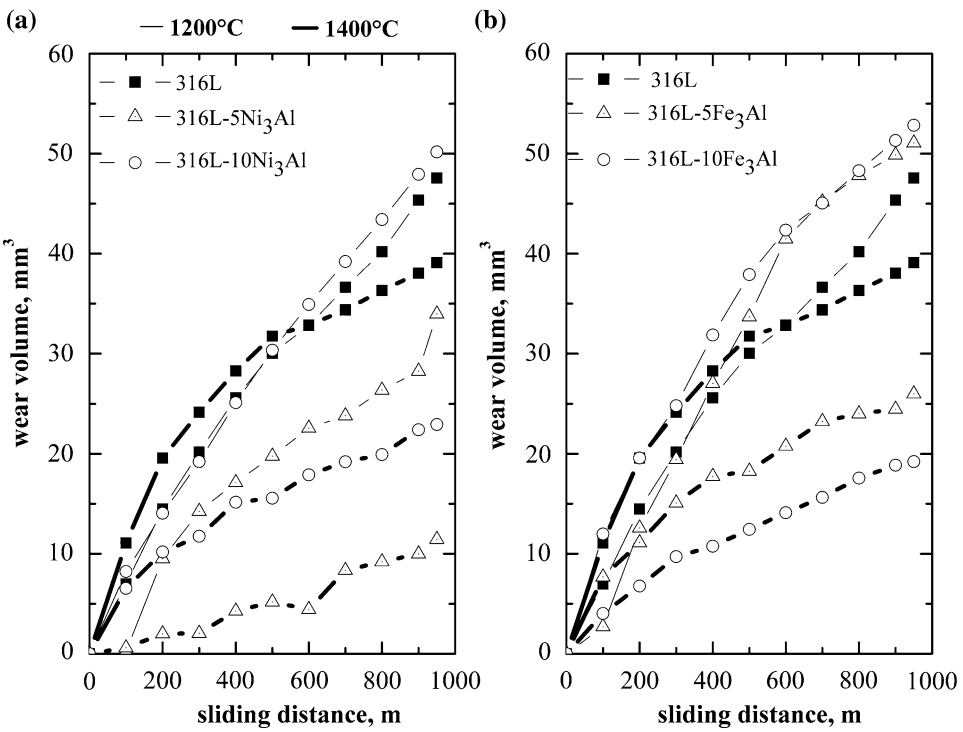

Fig. 7 Variation of the wear volume loss with sliding distance for sintered **a** Ni_3Al and **b** Fe_3Al added 316L stainless steel composites. The light and dark lines correspond to solid-state (1200 °C) and supersolidus sintered (1400 °C) compacts, respectively

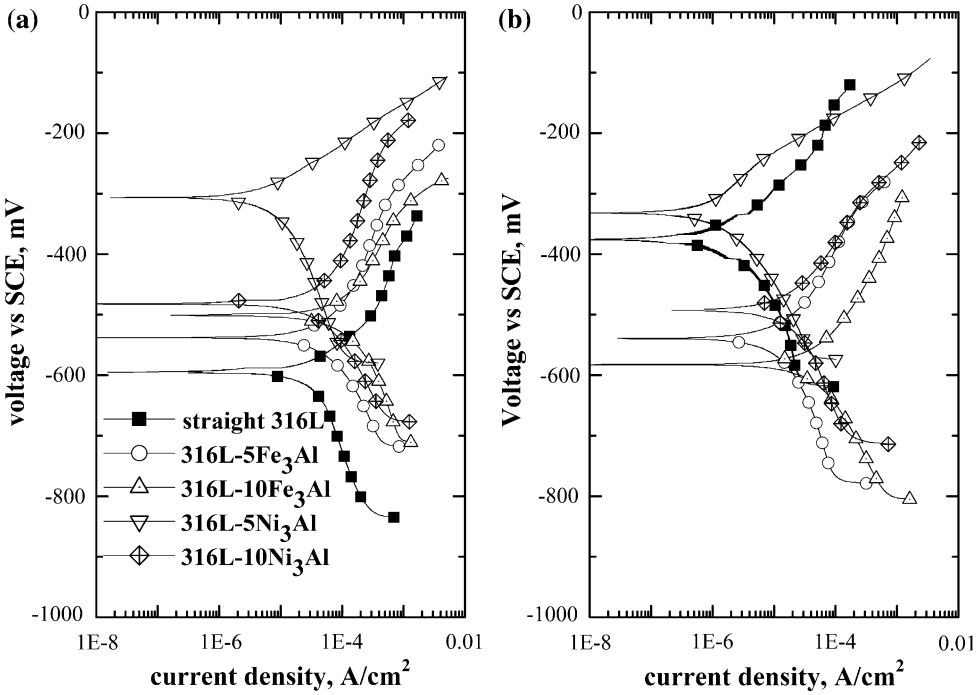

Fig. 9 Tafel curves for the straight 316L stainless steels and 316L–aluminide composites sintered at **a** 1200 °C and **b** 1400 °C

Table 3 Tafel extrapolation results of the sintered 316L–aluminide composites

Composition	Sintering temperature (°C)	β (mV/decade)		i_{corr} (μA/cm^2)	E_{corr} (mV)	Corrosion rate (mmpy)
		β_a	β_c			
316L	1200	93.30	280.7	35.9	−595	0.380
	1400	152.8	284.3	4.25	−368	0.045
316L–5Ni_3Al	1200	87.0	271.7	10.2	−302	0.108
	1400	256.4	198.9	2.82	−331	0.030
316L–10Ni_3Al	1200	366.5	238.3	83.4	−483	0.888
	1400	179.7	280.1	26.4	−492	0.281
316L–5Fe_3Al	1200	397.8	324.7	136	−539	1.452
	1400	240.5	436.2	27.4	−542	0.293
316L–10Fe_3Al	1200	392.9	426.7	304	−500	3.277
	1400	199	222.2	67.8	−585	0.731

steels deteriorate the corrosion resistance as compared to the straight 316L stainless steels sintered at similar conditions. However, supersolidus sintered aluminide added composites showed comparable corrosion rates as that of the solid-state sintered straight 316L stainless steels.

Conclusions

The present study investigates the effect of aluminide addition on the sintering behavior of austenitic stainless steel (316L) compacts. The compacts were sintered in solid-state (1200 °C) and supersolidus (1400 °C) condition. As compared to solid-state sintering, supersolidus sintering enhances densification in both straight 316L stainless steels as well as 316L–aluminide composites. The overall mechanical, tribological, and corrosion performance of straight 316L stainless steel and 316L reinforced with Ni_3Al and Fe_3Al correspondingly improves with increase in the sintering temperature. This has been correlated to the microstructure and the interaction between the stainless steel and aluminide additives in supersolidus sintered condition.

References

1. Shankar J, Upadhyaya A, Balasubramaniam R (2004) Corr Sci 46:487
2. Jain J, Kar AM, Upadhyaya A (2004) Mater Lett 58:2037
3. German RM (1985) Liquid phase sintering. Plenum Press, New York

4. Cambal L, Lund JA (1972) Int J Powder Metall 8(3):131
5. German RM (1997) Metall Mater Trans A 28A:1553
6. Pagounis E, Lindroos VK (1998) Mater Sci Eng A 246:221
7. Datta P, Upadhyaya GS (2003) Sci Sintering 32:109
8. Velasco F, Anton N, Torralba JM, Ruiz-Prieto JM (1997) Mater Sci Technol 13:847
9. Vardavoulias M, Jeandin M, Velasco F, Torralba JM (1996) Tribol Int 29:506
10. Akhtar F, Guo SJ (2008) Mater Char 59:84
11. Tjong SC, Lau KC (1999) Mater Lett 41:153
12. Tjong SC, Lau KC (2000) Comp Sci Tech 60:1141
13. Shankar J, Upadhyaya A, Balasubramaniam R (2002) Advances in powder metallurgy and particulate materials, vol 13. Princeton, p 313
14. Balaji S, Upadhyaya A (2007) Mater Chem Phys 101:310
15. Velasco F, Lima WM, Anton N, Abenojar J, Torralba JM (2003) Tribol Int 36:547
16. Abenojar J, Velasco F, Bautista A, Campos M, Bas JA, Torralba JM (2003) Compos Sci Technol 63:69
17. Abenojar J, Velasco F, Torralba JM, Bas JA, Calero JA (2002) Mater Sci Eng A 335:1
18. Balaji S, Vijay P, Upadhyaya A (2007) Scripta Mater 56:1063
19. Panda SS, Singh V, Upadhyaya A, Agrawal D (2006) Metall Mater Trans A 37A:2253
20. Kameo K, Friedrich K, Bartolomé JF, Díaz M, Esteban SL, Moya JS (2003) J Eur Ceram Soc 23:2867
21. Balasubramaniam R (2002) J Alloys Compd 330:506
22. Sedriks AJ (1979) Corrosion of stainless steels, 1st edn. John Wiley & Sons, New York, NY, p 52